

CERN-EP-2016-229
19 Sep 2016

Anomalous evolution of the near-side jet peak shape in Pb–Pb collisions at $\sqrt{s_{\text{NN}}} = 2.76 \text{ TeV}$

ALICE Collaboration*

Abstract

The measurement of two-particle angular correlations is a powerful tool to study jet quenching in a p_T region inaccessible by direct jet identification. In these measurements pseudorapidity ($\Delta\eta$) and azimuthal ($\Delta\phi$) differences are used to extract the shape of the near-side peak formed by particles associated to a higher p_T trigger particle ($1 < p_{T,\text{trig}} < 8 \text{ GeV}/c$). A combined fit of the near-side peak and long-range correlations is applied to the data allowing the extraction of the centrality evolution of the peak shape in Pb–Pb collisions at $\sqrt{s_{\text{NN}}} = 2.76 \text{ TeV}$. A significant broadening of the peak in the $\Delta\eta$ direction at low p_T is found from peripheral to central collisions, which vanishes above $4 \text{ GeV}/c$, while in the $\Delta\phi$ direction the peak is almost independent of centrality. For the 10% most central collisions and $1 < p_{T,\text{assoc}} < 2 \text{ GeV}/c$, $1 < p_{T,\text{trig}} < 3 \text{ GeV}/c$ a novel feature is observed: a depletion develops around the centre of the peak. The results are compared to pp collisions at the same centre of mass energy and to AMPT model simulations. The comparison to the investigated models suggests that the broadening and the development of the depletion is connected to the strength of radial and longitudinal flow.

*See Appendix A for the list of collaboration members

In elementary interactions with large momentum transfer ($Q^2 \gg \Lambda_{\text{QCD}}^2$), partons with high transverse momentum (p_T) are produced. They evolve from high to low virtuality producing parton showers and eventually hadronizing into a spray of collimated hadrons called jets. In interactions between heavy-ions, such high- p_T partons are produced at the early stages of the collisions. They propagate through the dense and hot medium created in these collisions and are expected to lose energy due to induced gluon radiation and elastic scatterings, a process commonly referred to as jet quenching. Correspondingly, an inclusive jet suppression has been observed at the LHC [1–3] together with a large di-jet energy asymmetry [4, 5], while studies of the momentum and angular distributions of jet fragments show only a small modification of the jet core [6–8], and an excess of soft particles radiated to large angles from the jet axis [9]. Semi-inclusive hadron–jet correlations show a suppression of recoil jet yield, with no in-medium modification of transverse jet structure observed [10].

Di-hadron angular correlations represent a powerful complementary tool to study jet modifications on a statistical basis in an energy region where jets cannot be identified event-by-event over the fluctuating background. Such studies involve measuring the distributions of the relative azimuthal angle $\Delta\varphi$ and pseudorapidity $\Delta\eta$ between particle pairs consisting of a trigger particle in a certain transverse momentum $p_{T,\text{trig}}$ interval and an associated particle in a $p_{T,\text{assoc}}$ interval. In these correlations, jet production manifests itself as a peak centred around ($\Delta\varphi = 0$, $\Delta\eta = 0$) (near-side peak) and a structure elongated in $\Delta\eta$ at $\Delta\varphi = \pi$ (the away-side or recoil-region). At low p_T , resonance decays as well as femtoscopic correlations also contribute to the near-side peak. The advantage of using di-hadron correlations is that an event-averaged subtraction of the background from particles uncorrelated to the jet can be performed. This advantage is shared with the analysis of hadron–jet correlations recently reported in Ref. [9, 10].

At RHIC, the near-side particle yield and peak shape of di-hadron correlations have been studied for different systems and collision energies [11–13]. Small modifications of the yields with respect to a pp reference from PYTHIA are observed and there is remarkably little dependence on the collision system at the centre-of-mass energies of $\sqrt{s_{\text{NN}}} = 62.4$ and 200 GeV. An exception is the measurement in central Au–Au collisions at $\sqrt{s_{\text{NN}}} = 200$ GeV where the jet-like correlation is substantially broader and the momentum spectrum softer than in peripheral collisions and than those in collisions of other systems in this kinematic regime. At the LHC, the measurement of the yield of particles associated to a high- p_T trigger particle (8–15 GeV/c) in central Pb–Pb collisions relative to the pp reference at $p_{T,\text{assoc}} > 3$ GeV/c shows a suppression on the away-side and a moderate enhancement on the near-side indicating that medium-induced modifications can also be expected on the near side [14]. Much stronger modifications are observed for lower trigger and associated particle p_T ($3 < p_{T,\text{trig}} < 3.5$ GeV/c and $1 < p_{T,\text{assoc}} < 1.5$ GeV/c) [15, 16]. In the most central Pb–Pb collisions, the near-side yield is enhanced by a factor of 1.7. The present paper expands these studies at the LHC to the characterisation of the angular distribution of the associated particles with respect to the trigger particle. The angular distribution is sensitive to the broadening of the jet due to its energy loss and the distribution of radiated energy. Moreover, possible interactions of the parton shower with the collective longitudinal expansion [17–19] or with turbulent colour fields [20] in the medium would result in near-side peak shapes that are broader in the $\Delta\eta$ than in the $\Delta\varphi$ direction. Results from the study of the near-side peak shape of charged particles as a function of centrality and for different combinations of trigger and associated particle p_T are discussed.

The data presented in this paper were taken by the ALICE detector, of which a detailed description can be found in Ref. [21]. The main subsystems used in the present analysis are the Inner Tracking System (ITS), and the Time Projection Chamber (TPC). These have a common acceptance of $|\eta| < 0.9$. The ITS consists of six layers of silicon detectors for vertex finding, tracking and triggering. The TPC is the main tracking detector measuring up to 159 space points per track. The V0 detector, two arrays of 32 scintillator tiles each, covering $2.8 < \eta < 5.1$ (V0-A) and $-3.7 < \eta < -1.7$ (V0-C), was used for triggering and centrality determination. All these detector systems have full azimuthal coverage.

Data from the 2010 and 2011 Pb–Pb runs of the LHC at $\sqrt{s_{\text{NN}}} = 2.76 \text{ TeV}$ and the 2011 pp run at the same energy are combined in the present analysis. In total, about 39 million Pb–Pb and 30 million pp events are used. Details about the trigger and event selection in Pb–Pb (pp) collisions can be found in Ref. [22] (Ref. [23]), while the centrality determination is described in Ref. [24].

The collision-vertex position is determined with tracks reconstructed in the ITS and TPC [25], and its value in the beam direction (z_{vtx}) is required to be within 7 cm of the detector centre. The Pb–Pb analysis is performed in the centrality classes 0–10% (most central), 10–20%, 20–30%, 30–50% and 50–80%. The analysis uses tracks reconstructed in the ITS and TPC with $1 < p_{\text{T}} < 8 \text{ GeV}/c$ and in a fiducial region of $|\eta| < 0.8$. The track selection is described in Refs. [26, 27]. The efficiency and purity of the primary charged-particle selection are estimated from a Monte Carlo (MC) simulation using the HIJING 1.383 event generator [28] (for Pb–Pb) and the PYTHIA 6.4 event generator [29] with the tune Perugia-0 [30] (for pp) with particle transport through the detector using GEANT3 [31]. The combined efficiency and acceptance for the track reconstruction in $|\eta| < 0.8$ is about 82–85% at $p_{\text{T}} = 1 \text{ GeV}/c$, and decreases to about 76–80% at $p_{\text{T}} = 8 \text{ GeV}/c$ depending on collision system, data sample and event centrality. The contamination originating from secondary particles from weak decays and interactions in the detector material decreases from 2.5–4.5% to 0.5–1% in the p_{T} range from 1 to 8 GeV/c . The contribution from fake tracks is negligible. From these quantities a correction factor is computed as a function of η , p_{T} , z_{vtx} and event centrality which is applied as a weight for each trigger particle and particle pair in the analysis.

The correlation between two charged particles (denoted trigger and associated particle) is measured as a function of $\Delta\varphi$ (defined within $-\pi/2$ and $3\pi/2$) and $\Delta\eta$ [32]. The correlation is expressed in terms of the associated yield per trigger particle for intervals of $p_{\text{T,trig}}$ and $p_{\text{T,assoc}}$, measured as:

$$\frac{1}{N_{\text{trig}}} \frac{d^2N_{\text{assoc}}}{d\Delta\eta d\Delta\varphi} = \frac{S(\Delta\eta, \Delta\varphi)}{B(\Delta\eta, \Delta\varphi)} \quad (1)$$

where N_{trig} is the total number of trigger particles in the centrality class and $p_{\text{T,trig}}$ interval, ranging from 0.18 to 36 per event. The signal distribution $S(\Delta\eta, \Delta\varphi) = 1/N_{\text{trig}} d^2N_{\text{same}}/d\Delta\eta d\Delta\varphi$ is the associated yield per trigger particle for particle pairs from the same event. The background distribution $B(\Delta\eta, \Delta\varphi) = \alpha d^2N_{\text{mixed}}/d\Delta\eta d\Delta\varphi$ accounts for the acceptance and efficiency of pair reconstruction. It is constructed by correlating the trigger particles in one event with the associated particles from other events. The background distribution is scaled by a factor α which is chosen such that $B(0, 0)$ is unity for pairs where both particles travel in approximately the same direction (i.e. $\Delta\varphi \approx 0$, $\Delta\eta \approx 0$), and thus the efficiency and acceptance for the two particles are identical by construction.

A selection on the opening angle of the particle pairs is applied to both signal and background to avoid a bias due to the reduced efficiency for pairs with small opening angles. Furthermore, correlations induced by secondary particles from long-lived neutral-particle decays (K_s^0 and Λ) and γ -conversions are suppressed by rejecting pairs in the corresponding invariant mass region. A correction for the mild $\Delta\eta$ dependence of the structures in the two-particle correlation due to the minor dependence of particle production and anisotropic flow on pseudorapidity is performed. For further details on the analysis procedure, see the companion paper [33].

In order to characterize the near-side peak shape, a simultaneous fit of the peak, the combinatorial background and the long-range correlation background stemming from collective effects is performed. This exploits that in two-particle correlations the near-side peak is centred around $\Delta\varphi = 0$, $\Delta\eta = 0$, while long-range correlation structures are mostly independent of $\Delta\eta$ [34]. This strategy limits the analysis to the near side as the away-side peak is elongated in $\Delta\eta$. The fit function used is a combination of a constant, a generalized two-dimensional Gaussian function and $\cos(n\Delta\varphi)$ terms for $n = 2, 3, 4$.

$$F(\Delta\varphi, \Delta\eta) = C_1 + \sum_{n=2}^4 2V_{n\Delta} \cos(n\Delta\varphi) +$$

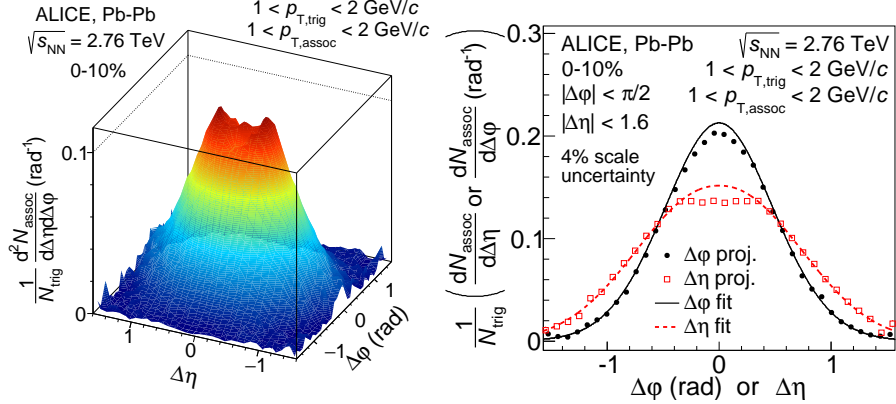


Fig. 1: Left panel: associated yield per trigger particle as a function of $\Delta\phi$ and $\Delta\eta$. The background obtained from the fit function has been subtracted in order to emphasize the near-side peak. Right panel projections to the $\Delta\phi$ and $\Delta\eta$ axes overlaid with the peak part of the fit function.

$$C_2 \cdot G_{\gamma_{\Delta\phi}, w_{\Delta\phi}}(\Delta\phi) \cdot G_{\gamma_{\Delta\eta}, w_{\Delta\eta}}(\Delta\eta) \quad (2)$$

$$G_{\gamma_x, w_x}(x) = \frac{\gamma_x}{2w_x \Gamma(1/\gamma_x)} \exp \left[-\left(\frac{|x|}{w_x} \right)^{\gamma_x} \right]. \quad (3)$$

Thus in Pb–Pb collisions, the background is characterized by four parameters ($C_1, V_{n\Delta}$) where $V_{n\Delta}$ are the Fourier components of the long-range correlations [35], and it should be noted that the inclusion of orders higher than four does not significantly change the fit results. In pp collisions, the background consists effectively only of the pedestal C_1 . The peak magnitude is characterized by C_2 , and the shape which is the focus of the present analysis by four parameters ($\gamma_{\Delta\phi}, w_{\Delta\phi}, \gamma_{\Delta\eta}, w_{\Delta\eta}$). The aim of using this fit function is to allow for a compact description of the data rather than attempting to give a physical meaning to each parameter. Therefore, the variance of G is calculated reducing the description of the peak shape to two parameters ($\sigma_{\Delta\phi}$ and $\sigma_{\Delta\eta}$). To describe the evolution of the peak shape from peripheral to central collisions the ratio of the width in the central bin (0–10%) and the peripheral bin (50–80%), denoted by $\sigma_{\Delta\phi}^{\text{CP}}$ and $\sigma_{\Delta\eta}^{\text{CP}}$, is also calculated.

In the data a depletion around $\Delta\phi = 0, \Delta\eta = 0$ is observed at low p_T , however, the fit function does not include such a depletion. To avoid a bias on the extracted peak width, some bins in the central region are excluded from the fit. The size of the excluded region varies with p_T and centrality (from no exclusion to 0.3). Thus, by definition, the peak width describes the shape of the peak outside of the central region. The central region is quantified below by computing the difference between the fit and the per-trigger yield within the exclusion region.

In Pb–Pb collisions, the obtained χ^2/ndf values of the fits are in the range 1.0–2.5; most are around 1.5. In the highest two p_T bins (i.e. in $3 < p_{T,\text{assoc}} < 8 \text{ GeV}/c$ and $4 < p_{T,\text{trig}} < 8 \text{ GeV}/c$) the values increase up to about 2.5 showing that at high p_T the peak shape starts to depart from the generalized Gaussian description. In pp collisions, the χ^2/ndf values are in the range 1.3–2.0.

Systematic uncertainties connected to the measurement are determined modifying the event and track selections. In addition, uncertainties related to the cut on pairs with small opening angles and neutral-particle decays, as well as the sensitivity to the pseudorapidity range are considered. The difference in the extracted parameters is studied as a function of p_T , centrality and collision system, but these dependencies are rather weak and one uncertainty value can be quoted for each type of systematic uncertainty in most cases. Finally, the different sources of systematic uncertainties are added in quadrature. The extracted peak widths are rather insensitive to changes in the selections (total uncertainty of about 2–4.5%), while the near-side depletion yield is more sensitive (about 24–45% uncertainty). The contribution from resonance decays was studied by performing the analysis separately for like and unlike sign pairs, and a

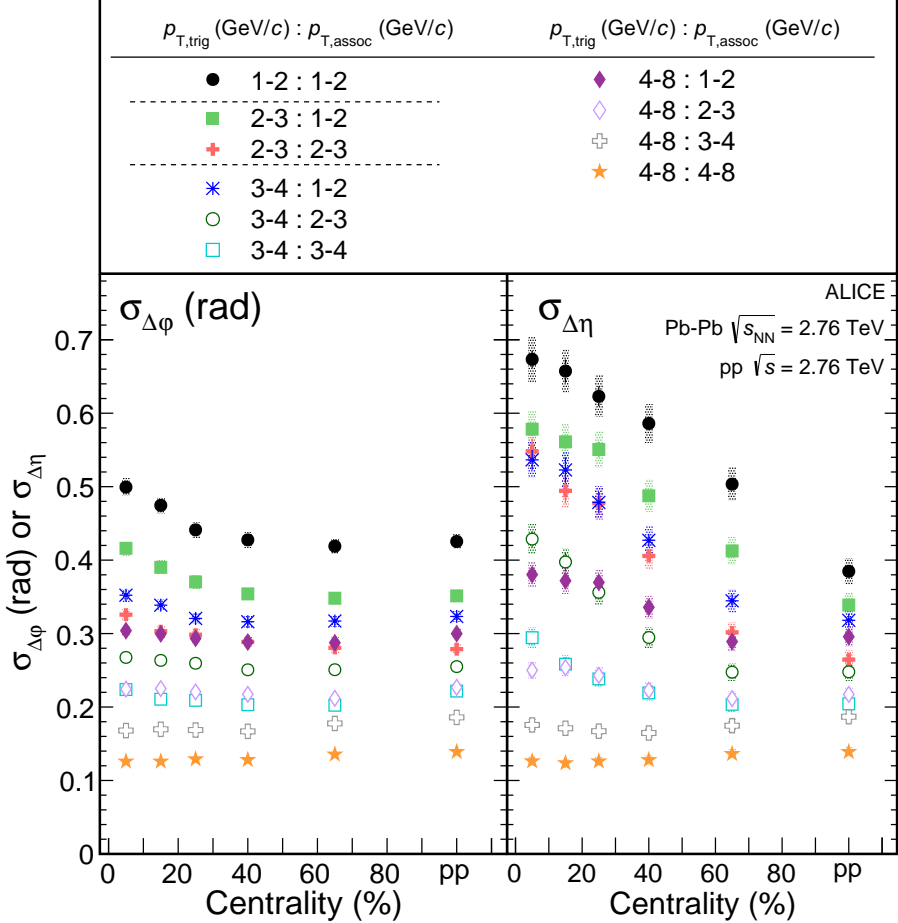


Fig. 2: Shape parameters $\sigma_{\Delta\phi}$ (left panel) and $\sigma_{\Delta\eta}$ (right panel) as a function of centrality in different p_T ranges. Lines indicate statistical uncertainties (mostly smaller than the marker size), while boxes denote systematic uncertainties. The markers are placed at the centre of the centrality bins.

significant influence on the results presented below was excluded.

Figure 1 shows the near-side peak in $1 < p_{T,\text{trig}} < 2 \text{ GeV}/c$ and $1 < p_{T,\text{assoc}} < 2 \text{ GeV}/c$ in the 10% most central collisions. In addition to the two-dimensional representation, projections are shown where the background estimated with Eq. 2 has been subtracted. The near-side peak is asymmetric, i.e. wider in $\Delta\eta$ than in $\Delta\phi$ as well as broader than in peripheral Pb–Pb collisions and pp collisions where it is mostly symmetric in $\Delta\phi$ and $\Delta\eta$ (not shown, see Ref. [33]). Furthermore, a depletion around $\Delta\phi = 0, \Delta\eta = 0$ develops which will be discussed in more detail further below. At higher p_T , the near-side peak is also found broader in central collisions than in peripheral or pp collisions although it is less pronounced, but the asymmetry disappears at the two highest p_T bins, see Ref. [33].

The extracted shape parameters $\sigma_{\Delta\phi}$ and $\sigma_{\Delta\eta}$ are presented in Fig. 2. In pp collisions, the σ values range from about 0.14 to about 0.43 showing the p_T dependence qualitatively expected due to the boost of the evolving parton shower: at larger p_T the peak is narrower. In the $\Delta\phi$ direction (left panel) the values obtained in pp collisions are consistent with those in peripheral Pb–Pb collisions. The peak width increases towards central events, which is most pronounced in the lowest p_T bin (20% increase). In the higher p_T bins no significant width increase can be observed. In the $\Delta\eta$ direction (right panel) a much larger broadening towards central collisions is found. Already in peripheral collisions the width is larger than in pp collisions. From peripheral to central collisions the width increases further up to $\sigma_{\Delta\eta} = 0.67$ in the lowest p_T bin and the largest relative increase of about 85% is observed for $2 < p_{T,\text{trig}} < 3 \text{ GeV}/c$ and $2 < p_{T,\text{assoc}} < 3 \text{ GeV}/c$. For all but the two largest p_T bins a significant broadening can be observed.

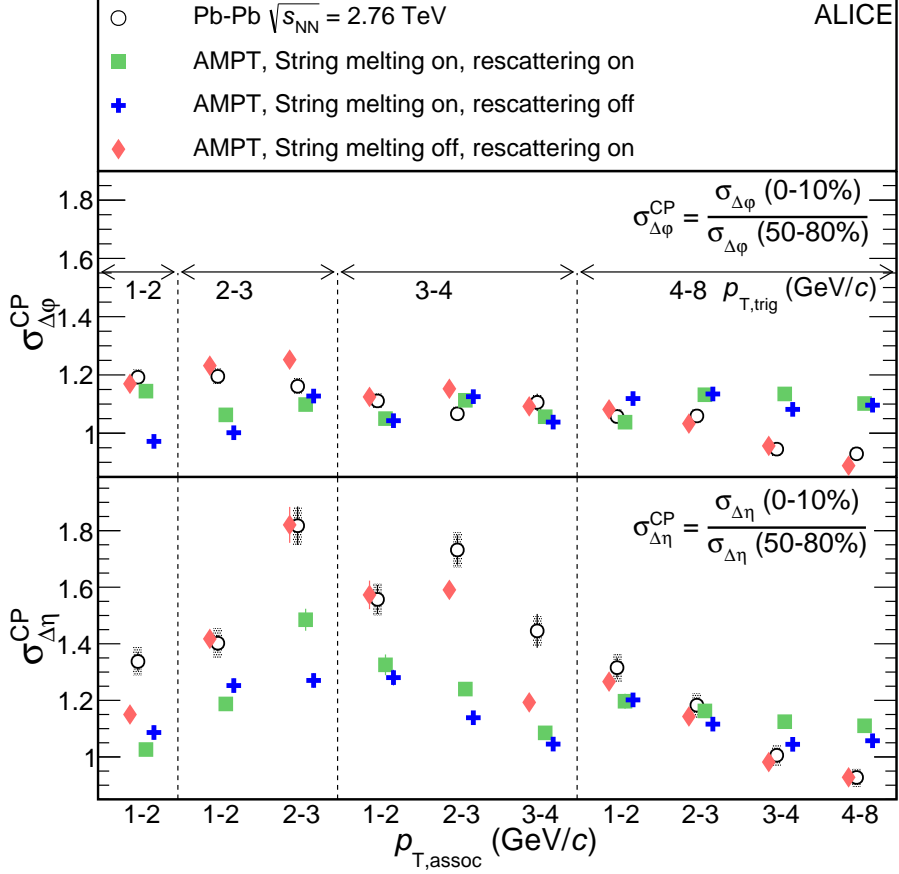


Fig. 3: Ratio of the peak widths in $\Delta\phi$ (top) and $\Delta\eta$ (bottom) observed in central (0–10%) and peripheral (50–80%) collisions as a function of $p_{T,\text{trig}}$ and $p_{T,\text{assoc}}$ ranges. The data is compared to different AMPT settings. Note that the x -axis combines the $p_{T,\text{assoc}}$ and $p_{T,\text{trig}}$ axis, and therefore, a uniform trend of the values is not expected.

This increase is quantified for all p_T bins in Fig. 3 by $\sigma_{\Delta\phi}^{\text{CP}}$ and $\sigma_{\Delta\eta}^{\text{CP}}$. The increase is quantified with respect to peripheral Pb–Pb instead of pp collisions to facilitate the MC comparisons discussed below.

In pp collisions, the peak shows circular symmetry in the $\Delta\eta$ – $\Delta\phi$ plane for all p_T . In Pb–Pb collisions, the peak becomes asymmetric towards central collisions for all but the two highest p_T bins. The magnitude of this asymmetry depends on p_T and is largest with about 70% ($\sigma_{\Delta\eta} > \sigma_{\Delta\phi}$) in the range $2 < p_{T,\text{assoc}} < 3 \text{ GeV}/c$ and $2 < p_{T,\text{trig}} < 3 \text{ GeV}/c$. These results are compatible with a similar study by the STAR collaboration at $\sqrt{s_{\text{NN}}} = 200 \text{ GeV}$ [12], which is detailed in the companion paper [33].

In Ref. [17] it was suggested that the interplay of longitudinal flow with a fragmenting high p_T parton can lead to the observed asymmetric peak shape. The authors argue that hard partons are interacting with a medium which shows collective behaviour, contrary to the simpler picture where the parton propagates through an isotropic medium with respect to the parton direction. In their calculation the scattering centres are Lorentz-boosted by applying a momentum shift depending on the collective component transverse to the parton-propagation direction. The calculation in Ref. [17] for Au–Au collisions at $\sqrt{s_{\text{NN}}} = 200 \text{ GeV}$ expects a 20% increase from peripheral to central events for the $\Delta\phi$ direction and a 60% increase for the $\Delta\eta$ direction. Despite the different centre of mass energy and collision system, the calculation is in quantitative agreement with the results presented in this paper.

In order to study further the possibility that an interplay of flow and jets can cause the observation, the data is compared to results from A Multi-Phase Transport model (AMPT) [36, 37]. Two mechanisms in AMPT produce collective effects: partonic and hadronic rescattering. Before partonic rescattering, the initially produced strings may be broken into smaller pieces by the so-called string melting. Three

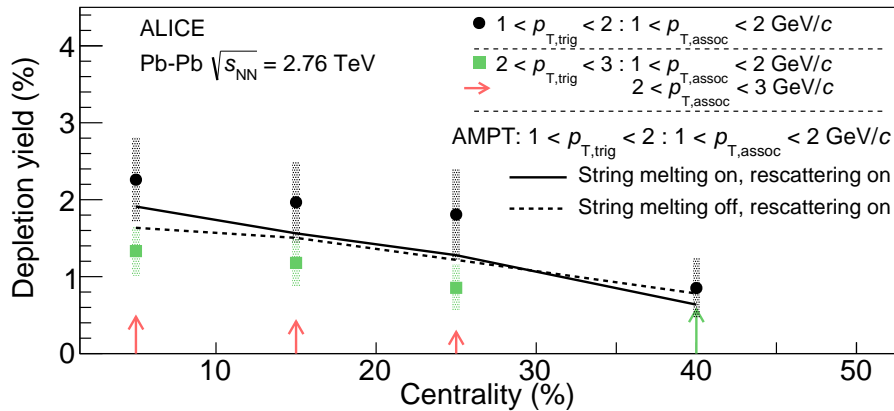


Fig. 4: Missing yield in the depletion region relative to the overall peak yield extracted from the fit. The arrows indicate the upper limit in case the uncertainty bands touch 0. For comparison, the non-zero values from two AMPT simulations are shown as lines.

different AMPT settings are considered which have either string melting (configuration (a)) or hadronic rescattering (b) or both activated (c) [38].

The peak widths are extracted from particle-level AMPT simulations in the same way as for the data. None of the AMPT settings provides an accurate description of the measured absolute widths. Further discussion and the corresponding figure can be found in Ref. [33]. In order to provide nevertheless a meaningful comparison of the relative increase, $\sigma_{\Delta\phi}^{\text{CP}}$ and $\sigma_{\Delta\eta}^{\text{CP}}$ from the models are shown together with the data in Fig. 3. In the $\Delta\phi$ direction, the setting with string melting deactivated and hadronic rescattering active follows the trend of the data closest. The two other settings show a more uniform distribution across p_T and only differ in the two lowest p_T bins. In the $\Delta\eta$ direction, the setting with string melting deactivated and hadronic rescattering active quite remarkably follows the trend of the data including the large increase for intermediate p_T . The two other settings show qualitatively a similar trend but miss the data quantitatively.

The presented results have focused up to now on the overall shape of the near-side peak. In addition to the broadening a distinct feature is observed, a depletion around $\Delta\phi = 0$, $\Delta\eta = 0$ (see Fig. 1). An extensive set of studies was carried out to exclude that this depletion could arise from a detector effect. A similar structure is found in AMPT simulations with hadronic rescattering regardless of the string melting setting [33].

In order to quantify this depletion, the difference between the fit (where the depletion region has been excluded, see above) and the per-trigger yield relative to the total peak yield for the p_T bins is computed and this is referred to as depletion yield in the following. The region where effects are expected from the limited two-track reconstruction efficiency ($|\Delta\phi| < 0.04$ and $|\Delta\eta| < 0.05$, which corresponds to 0.5–6% of the integrated region) is excluded from this calculation. Fig. 4 presents the depletion yield as a function of centrality for the p_T bins, where it is different from 0. It can be seen that $(2.2 \pm 0.5)\%$ of the yield is missing in the lowest p_T bin and in the 10% most central events. This value decreases gradually with centrality and with p_T . No significant depletion yield is observed for 50–80% (30–80%) centrality or pp collisions for the lowest (second lowest) p_T range. The depletion observed in the AMPT events is present only in the lowest p_T bin, where its value is compatible with the data for both settings where hadronic rescattering is switched on. For larger p_T bins and for the configuration without hadronic rescattering the depletion yield is consistent with 0 in AMPT.

The reported results are interpreted in the context of radial and anisotropic flow by calculating the radial-flow expansion velocity β_T and the elliptic flow coefficient $v_2\{2\}$ from the 10% most central events from data and from the AMPT samples. The expansion velocity β_T is extracted from a Blast-Wave fit to the

p_T -spectra of π , K and p in the rapidity range of $|y| < 0.5$ [39]. The $v_2\{2\}$ is extracted from two-particle correlations within $|\eta| < 0.8$ and $0.2 < p_T < 5 \text{ GeV}/c$ [40].

The depletion (Fig. 4) occurs in the two AMPT configurations where the β_T is large (0.442 (configuration (c)) and 0.540 (b)), while the configuration without the depletion has the smallest β_T (0.202 (a)). The coefficient $v_2\{2\}$ has significantly different values in the two configurations with depletion (3.30 (b) and 4.12 (c)), and the relative increase of the peak width (Fig. 3) is best described by the AMPT configuration with the largest β_T (b). Based on these studies, it seems that the radial flow rather than the elliptic flow may be responsible for the depletion and the broadening observed in the data.

In summary, we have presented a detailed characterization of the flow-subtracted near-side peak in two-particle correlations in Pb–Pb collisions at $\sqrt{s_{NN}} = 2.76 \text{ TeV}$ together with a measurement in pp collisions at the same energy. The near-side peak shows several untypical characteristics in Pb–Pb collisions: the peak gets broader and asymmetric from peripheral to central collisions over a wide p_T range, and an unexpected depletion develops in central collisions at low p_T . The broadening is present both in the $\Delta\varphi$ and the $\Delta\eta$ directions, but is significantly stronger for the $\Delta\eta$ direction, leading to the asymmetric shape of the peak. The near-side peak also shows the characteristic p_T dependence in both Pb–Pb and pp collisions.

AMPT simulations show also an asymmetric broadening, and the depletion is present when hadronic rescattering is included. The AMPT configuration with hadronic rescattering and without string melting reproduces quantitatively the relative peak broadening as well as the size of the depletion, underlining the importance of the hadronic phase in heavy-ion collisions. The extraction of the radial-flow expansion velocity suggests that the stronger the radial flow, the stronger the observed effects are. In addition, earlier theoretical and phenomenological work connected the longitudinal broadening of the near-side jet-like peak to strong longitudinal flow in AMPT [41], as well as to an interplay of partons traversing the longitudinally expanding medium [17]. Thus a possible scenario is that the presented observations are caused by the interplay of the jet with the collective expansion.

Acknowledgements

The ALICE Collaboration would like to thank all its engineers and technicians for their invaluable contributions to the construction of the experiment and the CERN accelerator teams for the outstanding performance of the LHC complex. The ALICE Collaboration gratefully acknowledges the resources and support provided by all Grid centres and the Worldwide LHC Computing Grid (WLCG) collaboration. The ALICE Collaboration acknowledges the following funding agencies for their support in building and running the ALICE detector: A. I. Alikhanyan National Science Laboratory (Yerevan Physics Institute) Foundation (ANSL), State Committee of Science and World Federation of Scientists (WFS), Armenia; Austrian Academy of Sciences and Nationalstiftung für Forschung, Technologie und Entwicklung, Austria; , Conselho Nacional de Desenvolvimento Científico e Tecnológico (CNPq), Financiadora de Estudos e Projetos (Finep) and Fundação de Amparo à Pesquisa do Estado de São Paulo (FAPESP), Brazil; Ministry of Education of China (MOE of China), Ministry of Science & Technology of China (MOST of China) and National Natural Science Foundation of China (NSFC), China; Ministry of Science, Education and Sport and Croatian Science Foundation, Croatia; Centro de Investigaciones Energéticas, Medioambientales y Tecnológicas (CIEMAT), Cuba; Ministry of Education, Youth and Sports of the Czech Republic, Czech Republic; Danish National Research Foundation (DNRF), The Carlsberg Foundation and The Danish Council for Independent Research — Natural Sciences, Denmark; Helsinki Institute of Physics (HIP), Finland; Commissariat à l’Energie Atomique (CEA) and Institut National de Physique Nucléaire et de Physique des Particules (IN2P3) and Centre National de la Recherche Scientifique (CNRS), France; Bundesministerium für Bildung, Wissenschaft, Forschung und Technologie (BMBF) and GSI Helmholtzzentrum für

Schwerionenforschung GmbH, Germany; Ministry of Education, Research and Religious Affairs, Greece; National Research, Development and Innovation Office, Hungary; Department of Atomic Energy Government of India (DAE), India; Indonesian Institute of Science, Indonesia; Centro Fermi - Museo Storico della Fisica e Centro Studi e Ricerche Enrico Fermi and Istituto Nazionale di Fisica Nucleare (INFN), Italy; Institute for Innovative Science and Technology , Nagasaki Institute of Applied Science (IIST), Japan Society for the Promotion of Science (JSPS) KAKENHI and Japanese Ministry of Education, Culture, Sports, Science and Technology (MEXT), Japan; Consejo Nacional de Ciencia (CONACYT) y Tecnología, through Fondo de Cooperación Internacional en Ciencia y Tecnología (FONCICYT) and Dirección General de Asuntos del Personal Académico (DGAPA), Mexico; Nationaal instituut voor subatomaire fysica (Nikhef), Netherlands; The Research Council of Norway, Norway; Commission on Science and Technology for Sustainable Development in the South (COMSATS), Pakistan; Pontificia Universidad Católica del Perú, Peru; Ministry of Science and Higher Education and National Science Centre, Poland; Ministry of Education and Scientific Research, Institute of Atomic Physics and Romanian National Agency for Science, Technology and Innovation, Romania; Joint Institute for Nuclear Research (JINR), Ministry of Education and Science of the Russian Federation and National Research Centre Kurchatov Institute, Russia; Ministry of Education, Science, Research and Sport of the Slovak Republic, Slovakia; National Research Foundation of South Africa, South Africa; Korea Institute of Science and Technology Information and National Research Foundation of Korea (NRF), South Korea; Centro de Investigaciones Energéticas, Medioambientales y Tecnológicas (CIEMAT) and Ministerio de Ciencia e Innovacion, Spain; Knut & Alice Wallenberg Foundation (KAW) and Swedish Research Council (VR), Sweden; European Organization for Nuclear Research, Switzerland; National Science and Technology Development Agency (NSDTA), Office of the Higher Education Commission under NRU project of Thailand and Suranaree University of Technology (SUT), Thailand; Turkish Atomic Energy Agency (TAEK), Turkey; National Academy of Sciences of Ukraine, Ukraine; Science and Technology Facilities Council (STFC), United Kingdom; National Science Foundation of the United States of America (NSF) and United States Department of Energy, Office of Nuclear Physics (DOE NP), United States.

References

- [1] **ATLAS** Collaboration, G. Aad *et al.*, “Measurement of the jet radius and transverse momentum dependence of inclusive jet suppression in lead-lead collisions at $\sqrt{s_{NN}} = 2.76$ TeV with the ATLAS detector,” *Phys. Lett.* **B719** (2013) 220–241, arXiv:1208.1967 [hep-ex].
- [2] **ALICE** Collaboration, B. Abelev *et al.*, “Measurement of charged jet suppression in Pb-Pb collisions at $\sqrt{s_{NN}} = 2.76$ TeV,” *JHEP* **03** (2014) 013, arXiv:1311.0633 [nucl-ex].
- [3] **ALICE** Collaboration, J. Adam *et al.*, “Measurement of jet suppression in central Pb-Pb collisions at $\sqrt{s_{NN}} = 2.76$ TeV,” *Phys. Lett.* **B746** (2015) 1–14, arXiv:1502.01689 [nucl-ex].
- [4] **ATLAS** Collaboration, G. Aad *et al.*, “Observation of a Centrality-Dependent Dijet Asymmetry in Lead-Lead Collisions at $\sqrt{s_{NN}} = 2.77$ TeV with the ATLAS Detector at the LHC,” *Phys. Rev. Lett.* **105** (2010) 252303, arXiv:1011.6182 [hep-ex].
- [5] **CMS** Collaboration, S. Chatrchyan *et al.*, “Observation and studies of jet quenching in PbPb collisions at nucleon-nucleon center-of-mass energy = 2.76 TeV,” *Phys. Rev.* **C84** (2011) 024906, arXiv:1102.1957 [nucl-ex].
- [6] **CMS** Collaboration, S. Chatrchyan *et al.*, “Measurement of jet fragmentation into charged particles in pp and PbPb collisions at $\sqrt{s_{NN}} = 2.76$ TeV,” *JHEP* **1210** (2012) 087, arXiv:1205.5872 [nucl-ex].

- [7] CMS Collaboration, S. Chatrchyan *et al.*, “Measurement of jet fragmentation in PbPb and pp collisions at $\sqrt{s_{NN}} = 2.76$ TeV,” *Phys. Rev.* **C90** (2014) 024908, arXiv:1406.0932 [nucl-ex].
- [8] ATLAS Collaboration, G. Aad *et al.*, “Measurement of inclusive jet charged-particle fragmentation functions in Pb+Pb collisions at $\sqrt{s_{NN}} = 2.76$ TeV with the ATLAS detector,” *Phys. Lett.* **B739** (2014) 320–342, arXiv:1406.2979 [hep-ex].
- [9] CMS Collaboration, V. Khachatryan *et al.*, “Correlations between jets and charged particles in PbPb and pp collisions at $\sqrt{s_{NN}} = 2.76$ TeV,” *JHEP* **02** (2016) 156, arXiv:1601.00079 [nucl-ex].
- [10] ALICE Collaboration, J. Adam *et al.*, “Measurement of jet quenching with semi-inclusive hadron-jet distributions in central Pb-Pb collisions at $\sqrt{s_{NN}} = 2.76$ TeV,” *JHEP* **09** (2015) 170, arXiv:1506.03984 [nucl-ex].
- [11] STAR Collaboration, B. I. Abelev *et al.*, “Long range rapidity correlations and jet production in high energy nuclear collisions,” *Phys. Rev.* **C80** (2009) 064912, arXiv:0909.0191 [nucl-ex].
- [12] STAR Collaboration, G. Agakishiev *et al.*, “System size and energy dependence of near-side di-hadron correlations,” *Phys. Rev.* **C85** (2012) 014903, arXiv:1110.5800 [nucl-ex].
- [13] STAR Collaboration, L. Adamczyk *et al.*, “Jet-Hadron Correlations in $\sqrt{s_{NN}} = 200$ GeV $p + p$ and Central $Au + Au$ Collisions,” *Phys. Rev. Lett.* **112** (2014) 122301, arXiv:1302.6184 [nucl-ex].
- [14] ALICE Collaboration, K. Aamodt *et al.*, “Particle-yield modification in jet-like azimuthal di-hadron correlations in Pb-Pb collisions at $\sqrt{s_{NN}} = 2.76$ TeV,” *Phys. Rev. Lett.* **108** (2012) 092301, arXiv:1110.0121 [nucl-ex].
- [15] CMS Collaboration, S. Chatrchyan *et al.*, “Centrality dependence of dihadron correlations and azimuthal anisotropy harmonics in Pb–Pb collisions at $\sqrt{s_{NN}} = 2.76$ TeV,” *Eur. Phys. J.* **C72** (2012) 2012, arXiv:1201.3158 [nucl-ex].
- [16] ALICE Collaboration, J. Adam *et al.*, “Jet-like correlations with neutral pion triggers in pp and central Pb-Pb collisions at 2.76 TeV,” arXiv:1608.07201 [nucl-ex].
- [17] N. Armesto, C. A. Salgado, and U. A. Wiedemann, “Measuring the collective flow with jets,” *Phys. Rev. Lett.* **93** (2004) 242301, arXiv:hep-ph/0405301.
- [18] N. Armesto, C. A. Salgado, and U. A. Wiedemann, “Low-p(T) collective flow induces high-p(T) jet quenching,” *Phys. Rev.* **C72** (2005) 064910, arXiv:hep-ph/0411341 [hep-ph].
- [19] P. Romatschke, “Momentum broadening in an anisotropic plasma,” *Phys. Rev.* **C75** (2007) 014901, arXiv:hep-ph/0607327 [hep-ph].
- [20] A. Majumder, B. Muller, and S. A. Bass, “Longitudinal Broadening of Quenched Jets in Turbulent Color Fields,” *Phys. Rev. Lett.* **99** (2007) 042301, arXiv:hep-ph/0611135 [hep-ph].
- [21] ALICE Collaboration, K. Aamodt *et al.*, “The ALICE experiment at the CERN LHC,” *JINST* **3** (2008) S08002.
- [22] ALICE Collaboration, K. Aamodt *et al.*, “Centrality dependence of the charged-particle multiplicity density at mid-rapidity in Pb-Pb collisions at $\sqrt{s_{NN}} = 2.76$ TeV,” *Phys. Rev. Lett.* **106** (2011) 032301, arXiv:1012.1657 [nucl-ex].

- [23] ALICE Collaboration, B. Abelev *et al.*, “Measurement of inelastic, single- and double-diffractive cross sections in proton–proton collisions at the LHC with ALICE,” *Eur. Phys. J.* **C73** (2013) 2456, arXiv:1208.4968 [hep-ex].
- [24] ALICE Collaboration, B. Abelev *et al.*, “Centrality determination of Pb–Pb collisions at $\sqrt{s_{\text{NN}}} = 2.76$ TeV with ALICE,” *Phys. Rev.* **C88** (2013) 044909, arXiv:1301.4361 [nucl-ex].
- [25] ALICE Collaboration, B. Abelev *et al.*, “Centrality Dependence of Charged Particle Production at Large Transverse Momentum in Pb–Pb Collisions at $\sqrt{s_{\text{NN}}} = 2.76$ TeV,” *Phys. Lett.* **B720** (2013) 52–62, arXiv:1208.2711 [hep-ex].
- [26] ALICE Collaboration, B. Abelev *et al.*, “Measurement of event background fluctuations for charged particle jet reconstruction in Pb–Pb collisions at $\sqrt{s_{\text{NN}}} = 2.76$ TeV,” *JHEP* **1203** (2012) 053, arXiv:1201.2423 [hep-ex].
- [27] ALICE Collaboration, B. Abelev *et al.*, “Underlying event measurements in pp collisions at $\sqrt{s} = 0.9$ and 7 TeV with the ALICE experiment at the LHC,” *JHEP* **1207** (2012) 116, arXiv:1112.2082 [hep-ex].
- [28] X.-N. Wang and M. Gyulassy, “HIJING: A Monte Carlo model for multiple jet production in pp, pA and AA collisions,” *Phys. Rev.* **D44** (1991) 3501.
- [29] T. Sjostrand, S. Mrenna, and P. Z. Skands, “PYTHIA 6.4 physics and manual,” *JHEP* **0605** (2006) 026, arXiv:hep-ph/0603175 [hep-ph].
- [30] P. Z. Skands, “Tuning Monte Carlo generators: The Perugia tunes,” *Phys. Rev.* **D82** (2010) 074018, arXiv:1005.3457 [hep-ph].
- [31] R. Brun *et al.*, “Geant detector description and simulation tool,” *CERN Program Library Long Write-up*, W5013 (1994).
- [32] ALICE Collaboration, B. Abelev *et al.*, “Long-range angular correlations on the near and away side in p–Pb collisions at $\sqrt{s_{\text{NN}}}=5.02$ TeV,” *Phys. Lett.* **B719** (2013) 29–41, arXiv:1212.2001 [nucl-ex].
- [33] ALICE Collaboration, J. Adam *et al.*, “Long version of this paper,” *Phys. Rev.* **C**.
- [34] ATLAS Collaboration, G. Aad *et al.*, “Measurement of the centrality and pseudorapidity dependence of the integrated elliptic flow in lead-lead collisions at $\sqrt{s_{\text{NN}}} = 2.76$ TeV with the ATLAS detector,” *Eur. Phys. J.* **C74** (2014) 2982, arXiv:1405.3936 [hep-ex].
- [35] ALICE Collaboration, K. Aamodt *et al.*, “Harmonic decomposition of two-particle angular correlations in Pb–Pb collisions at $\sqrt{s_{\text{NN}}} = 2.76$ TeV,” *Phys. Lett.* **B708** (2012) 249–264, arXiv:1109.2501 [nucl-ex].
- [36] Z.-W. Lin, C. M. Ko, B.-A. Li, B. Zhang, and S. Pal, “A Multi-phase transport model for relativistic heavy ion collisions,” *Phys. Rev.* **C72** (2005) 064901, arXiv:nucl-th/0411110 [nucl-th].
- [37] J. Xu and C. M. Ko, “Pb–Pb collisions at $\sqrt{s_{\text{NN}}} = 2.76$ TeV in a multiphase transport model,” *Phys. Rev.* **C83** (2011) 034904, arXiv:1101.2231 [nucl-th].
- [38] ALICE Collaboration, J. Adam *et al.*, “Higher harmonic flow coefficients of identified hadrons in Pb–Pb collisions at $\sqrt{s_{\text{NN}}} = 2.76$ TeV,” arXiv:1606.06057 [nucl-ex].

- [39] ALICE Collaboration, B. Abelev *et al.*, “Centrality dependence of π , K, p production in Pb-Pb collisions at $\sqrt{s_{NN}} = 2.76$ TeV,” *Phys. Rev.* **C88** (2013) 044910, arXiv:1303.0737 [hep-ex].
- [40] ALICE Collaboration, K. Aamodt *et al.*, “Elliptic flow of charged particles in Pb+Pb collisions at 2.76 TeV,” *Phys. Rev. Lett.* **105** (2010) 252302, arXiv:1011.3914 [nucl-ex].
- [41] G. L. Ma, S. Zhang, Y. G. Ma, X. Z. Cai, J. H. Chen, and C. Zhong, “Longitudinal broadening of near side jets due to parton cascade,” *Eur. Phys. J.* **C57** (2008) 589–593, arXiv:0807.3987 [nucl-th].

A The ALICE Collaboration

J. Adam³⁹, D. Adamová⁸⁶, M.M. Aggarwal⁹⁰, G. Aglieri Rinella³⁵, M. Agnello^{113,31}, N. Agrawal⁴⁸, Z. Ahammed¹³⁷, S. Ahmad¹⁸, S.U. Ahn⁷⁰, S. Aiola¹⁴¹, A. Akindinov⁵⁵, S.N. Alam¹³⁷, D.S.D. Albuquerque¹²⁴, D. Aleksandrov⁸², B. Alessandro¹¹³, D. Alexandre¹⁰⁴, R. Alfaro Molina⁶⁵, A. Alici^{107,12}, A. Alkin³, J. Alme^{22,37}, T. Alt⁴², S. Altinpinar²², I. Altsybeev¹³⁶, C. Alves Garcia Prado¹²³, M. An⁷, C. Andrei⁸⁰, H.A. Andrews¹⁰⁴, A. Andronic¹⁰⁰, V. Anguelov⁹⁶, C. Anson⁸⁹, T. Antičić¹⁰¹, F. Antinori¹¹⁰, P. Antonioli¹⁰⁷, R. Anwar¹²⁶, L. Aphecetche¹¹⁶, H. Appelshäuser⁶¹, S. Arcelli²⁷, R. Arnaldi¹¹³, O.W. Arnold^{97,36}, I.C. Arsene²¹, M. Arslanbekov⁶¹, B. Audurier¹¹⁶, A. Augustinus³⁵, R. Averbeck¹⁰⁰, M.D. Azmi¹⁸, A. Badalà¹⁰⁹, Y.W. Baek⁶⁹, S. Bagnasco¹¹³, R. Bailhache⁶¹, R. Bala⁹³, S. Balasubramanian¹⁴¹, A. Baldissari¹⁵, R.C. Baral⁵⁸, A.M. Barbano²⁶, R. Barbera²⁸, F. Barile³³, G.G. Barnaföldi¹⁴⁰, L.S. Barnby^{104,35}, V. Barret⁷², P. Bartalini⁷, K. Barth³⁵, J. Bartke^{120,i}, E. Bartsch⁶¹, M. Basile²⁷, N. Bastid⁷², S. Basu¹³⁷, B. Bathen⁶², G. Batigne¹¹⁶, A. Batista Camejo⁷², B. Batyunya⁶⁸, P.C. Batzing²¹, I.G. Bearden⁸³, H. Beck⁹⁶, C. Bedda³¹, N.K. Behera⁵¹, I. Belikov⁶⁶, F. Bellini²⁷, H. Bello Martinez², R. Bellwied¹²⁶, L.G.E. Beltran¹²², V. Belyaev⁷⁷, G. Bencedi¹⁴⁰, S. Beole²⁶, A. Bercuci⁸⁰, Y. Berdnikov⁸⁸, D. Berenyi¹⁴⁰, R.A. Bertens^{54,129}, D. Berziano³⁵, L. Betev³⁵, A. Bhasin⁹³, I.R. Bhat⁹³, A.K. Bhati⁹⁰, B. Bhattacharjee⁴⁴, J. Bhom¹²⁰, L. Bianchi¹²⁶, N. Bianchi⁷⁴, C. Bianchin¹³⁹, J. Bielčík³⁹, J. Bielčíková⁸⁶, A. Bilandžić^{36,97}, G. Biro¹⁴⁰, R. Biswas⁴, S. Biswas^{81,4}, S. Bjelogrlic⁵⁴, J.T. Blair¹²¹, D. Blau⁸², C. Blume⁶¹, F. Bock^{96,76}, A. Bogdanov⁷⁷, L. Boldizsár¹⁴⁰, M. Bombara⁴⁰, M. Bonora³⁵, J. Book⁶¹, H. Borel¹⁵, A. Borissov⁹⁹, M. Borri¹²⁸, E. Botta²⁶, C. Bourjau⁸³, P. Braun-Munzinger¹⁰⁰, M. Bregant¹²³, T.A. Broker⁶¹, T.A. Browning⁹⁸, M. Broz³⁹, E.J. Brucken⁴⁶, E. Bruna¹¹³, G.E. Bruno³³, D. Budnikov¹⁰², H. Buesching⁶¹, S. Bufalino^{26,31}, P. Buhler¹¹⁵, S.A.I. Buitron⁶³, P. Buncic³⁵, O. Busch¹³², Z. Buthelezi⁶⁷, J.B. Butt¹⁶, J.T. Buxton¹⁹, J. Cabala¹¹⁸, D. Caffarri³⁵, H. Caines¹⁴¹, A. Caliva⁵⁴, E. Calvo Villar¹⁰⁵, P. Camerini²⁵, F. Carena³⁵, W. Carena³⁵, F. Carnesecchi^{27,12}, J. Castillo Castellanos¹⁵, A.J. Castro¹²⁹, E.A.R. Casula²⁴, C. Ceballos Sanchez⁹, J. Cepila³⁹, P. Cerello¹¹³, J. Cerkala¹¹⁸, B. Chang¹²⁷, S. Chapelard³⁵, M. Chartier¹²⁸, J.L. Charvet¹⁵, S. Chattopadhyay¹³⁷, S. Chattopadhyay¹⁰³, A. Chauvin^{36,97}, V. Chelnokov³, M. Cherney⁸⁹, C. Cheshkov¹³⁴, B. Cheynis¹³⁴, V. Chibante Barroso³⁵, D.D. Chinellato¹²⁴, S. Cho⁵¹, P. Chochula³⁵, K. Choi⁹⁹, M. Chojnacki⁸³, S. Choudhury¹³⁷, P. Christakoglou⁸⁴, C.H. Christensen⁸³, P. Christiansen³⁴, T. Chujo¹³², S.U. Chung⁹⁹, C. Cicalo¹⁰⁸, L. Cifarelli^{12,27}, F. Cindolo¹⁰⁷, J. Cleymans⁹², F. Colamaria³³, D. Colella^{35,56}, A. Collu⁷⁶, M. Colocci²⁷, G. Conesa Balbastre⁷³, Z. Conesa del Valle⁵², M.E. Connors^{141,ii}, J.G. Contreras³⁹, T.M. Cormier⁸⁷, Y. Corrales Morales¹¹³, I. Cortés Maldonado², P. Cortese³², M.R. Cosentino^{125,123}, F. Costa³⁵, J. Crkovská⁵², P. Crochet⁷², R. Cruz Albino¹¹, E. Cuautle⁶³, L. Cunqueiro^{35,62}, T. Dahms^{36,97}, A. Dainese¹¹⁰, M.C. Danisch⁹⁶, A. Danu⁵⁹, D. Das¹⁰³, I. Das¹⁰³, S. Das⁴, A. Dash⁸¹, S. Dash⁴⁸, S. De^{123,49}, A. De Caro³⁰, G. de Cataldo¹⁰⁶, C. de Conti¹²³, J. de Cuveland⁴², A. De Falco²⁴, D. De Gruttola^{30,12}, N. De Marco¹¹³, S. De Pasquale³⁰, R.D. De Souza¹²⁴, A. Deisting^{100,96}, A. Deloff⁷⁹, C. Deplano⁸⁴, P. Dhankher⁴⁸, D. Di Bari³³, A. Di Mauro³⁵, P. Di Nezza⁷⁴, B. Di Ruzza¹¹⁰, M.A. Diaz Corchero¹⁰, T. Dietel⁹², P. Dillenseger⁶¹, R. Divià³⁵, Ø. Djupsland²², A. Dobrin^{84,35}, D. Domenicis Gimenez¹²³, B. Döningus⁶¹, O. Dordic²¹, T. Drozhzhova⁶¹, A.K. Dubey¹³⁷, A. Dubla¹⁰⁰, L. Ducroux¹³⁴, A.K. Duggal⁹⁰, P. Dupieux⁷², R.J. Ehlers¹⁴¹, D. Elia¹⁰⁶, E. Endress¹⁰⁵, H. Engel⁶⁰, E. Epple¹⁴¹, B. Erazmus¹¹⁶, F. Erhardt¹³³, B. Espagnon⁵², S. Esumi¹³², G. Eulisse³⁵, J. Eum⁹⁹, D. Evans¹⁰⁴, S. Evdokimov¹¹⁴, G. Eyyubova³⁹, L. Fabbietti^{36,97}, D. Fabris¹¹⁰, J. Faivre⁷³, A. Fantoni⁷⁴, M. Fasel^{76,87}, L. Feldkamp⁶², A. Feliciello¹¹³, G. Feofilov¹³⁶, J. Ferencei⁸⁶, A. Fernández Téllez², E.G. Ferreiro¹⁷, A. Ferretti²⁶, A. Festanti²⁹, V.J.G. Feuillard^{72,15}, J. Figiel¹²⁰, M.A.S. Figueredo¹²³, S. Filchagin¹⁰², D. Finogeev⁵³, F.M. Fionda²⁴, E.M. Fiore³³, M. Floris³⁵, S. Foertsch⁶⁷, P. Foka¹⁰⁰, S. Fokin⁸², E. Fragiacomo¹¹², A. Francescon³⁵, A. Francisco¹¹⁶, U. Frankenfeld¹⁰⁰, G.G. Fronze²⁶, U. Fuchs³⁵, C. Furret⁷³, A. Furs⁵³, M. Fusco Girard³⁰, J.J. Gaardhøje⁸³, M. Gagliardi²⁶, A.M. Gago¹⁰⁵, K. Gajdosova⁸³, M. Gallio²⁶, C.D. Galvan¹²², D.R. Gangadhara⁷⁶, P. Ganoti^{35,91}, C. Gao⁷, C. Garabatos¹⁰⁰, E. Garcia-Solis¹³, K. Garg²⁸, P. Garg⁴⁹, C. Gargiulo³⁵, P. Gasik^{36,97}, E.F. Gauger¹²¹, M.B. Gay Ducati⁶⁴, M. Germain¹¹⁶, P. Ghosh¹³⁷, S.K. Ghosh⁴, P. Gianotti⁷⁴, P. Giubellino^{113,35}, P. Giubilato²⁹, E. Gladysz-Dziadus¹²⁰, P. Glässel⁹⁶, D.M. Goméz Coral⁶⁵, A. Gomez Ramirez⁶⁰, A.S. Gonzalez³⁵, V. Gonzalez¹⁰, P. González-Zamora¹⁰, S. Gorbunov⁴², L. Görlich¹²⁰, S. Gotovac¹¹⁹, V. Grabski⁶⁵, L.K. Graczykowski¹³⁸, K.L. Graham¹⁰⁴, L. Greiner⁷⁶, A. Grelli⁵⁴, C. Grigoras³⁵, V. Grigoriev⁷⁷, A. Grigoryan¹, S. Grigoryan⁶⁸, N. Grion¹¹², J.M. Gronefeld¹⁰⁰, J.F. Grosse-Oetringhaus³⁵, R. Grossi¹⁰⁰, L. Gruber¹¹⁵, F. Guber⁵³, R. Guernane^{35,73}, B. Guerzoni²⁷, K. Gulbrandsen⁸³, T. Gunji¹³¹, A. Gupta⁹³, R. Gupta⁹³, I.B. Guzman², R. Haake^{35,62}, C. Hadjidakis⁵², H. Hamagaki^{131,78}, G. Hamar¹⁴⁰, J.C. Hamon⁶⁶, J.W. Harris¹⁴¹, A. Harton¹³, D. Hatzifotiadou¹⁰⁷, S. Hayashi¹³¹, S.T. Heckel⁶¹, E. Hellbär⁶¹, H. Helstrup³⁷, A. Hergelegiu⁸⁰, G. Herrera Corral¹¹, F. Herrmann⁶², B.A. Hess⁹⁵, K.F. Hetland³⁷, H. Hillemanns³⁵, B. Hippolyte⁶⁶, J. Hladky⁵⁷, D. Horak³⁹, R. Hosokawa¹³², P. Hristov³⁵, C. Hughes¹²⁹, T.J. Humanic¹⁹, N. Hussain⁴⁴, T. Hussain¹⁸, D. Hutter⁴², D.S. Hwang²⁰, R. Ilkaev¹⁰², M. Inaba¹³²,

M. Ippolitov^{82,77}, M. Irfan¹⁸, V. Isakov⁵³, M.S. Islam⁴⁹, M. Ivanov^{100,35}, V. Ivanov⁸⁸, V. Izucheev¹¹⁴, B. Jacak⁷⁶, N. Jacazio²⁷, P.M. Jacobs⁷⁶, M.B. Jadhav⁴⁸, S. Jadlovska¹¹⁸, J. Jadlovsky¹¹⁸, C. Jahnke^{123,36}, M.J. Jakubowska¹³⁸, M.A. Janik¹³⁸, P.H.S.Y. Jayarathna¹²⁶, C. Jena⁸¹, S. Jena¹²⁶, R.T. Jimenez Bustamante¹⁰⁰, P.G. Jones¹⁰⁴, A. Jusko¹⁰⁴, P. Kalinak⁵⁶, A. Kalweit³⁵, J.H. Kang¹⁴², V. Kaplin⁷⁷, S. Kar¹³⁷, A. Karasu Uysal⁷¹, O. Karavichev⁵³, T. Karavicheva⁵³, L. Karayan^{100,96}, E. Karpechev⁵³, U. Kebschull⁶⁰, R. Keidel¹⁴³, D.L.D. Keijdener⁵⁴, M. Keil³⁵, M. Mohisin Khan^{18,iii}, P. Khan¹⁰³, S.A. Khan¹³⁷, A. Khanzadeev⁸⁸, Y. Kharlov¹¹⁴, A. Khatun¹⁸, A. Khuntia⁴⁹, B. Kileng³⁷, D.W. Kim⁴³, D.J. Kim¹²⁷, D. Kim¹⁴², H. Kim¹⁴², J.S. Kim⁴³, J. Kim⁹⁶, M. Kim⁵¹, M. Kim¹⁴², S. Kim²⁰, T. Kim¹⁴², S. Kirsch⁴², I. Kisel⁴², S. Kiselev⁵⁵, A. Kisiel¹³⁸, G. Kiss¹⁴⁰, J.L. Klay⁶, C. Klein⁶¹, J. Klein³⁵, C. Klein-Bösing⁶², S. Klewin⁹⁶, A. Kluge³⁵, M.L. Knichel⁹⁶, A.G. Knospe^{121,126}, C. Kobdaj¹¹⁷, M. Kofarago³⁵, T. Kollegger¹⁰⁰, A. Kolojvari¹³⁶, V. Kondratiev¹³⁶, N. Kondratyeva⁷⁷, E. Kondratyuk¹¹⁴, A. Konevskikh⁵³, M. Kopcik¹¹⁸, M. Kour⁹³, C. Kouzinopoulos³⁵, O. Kovalenko⁷⁹, V. Kovalenko¹³⁶, M. Kowalski¹²⁰, G. Koyithatta Meethaleveedu⁴⁸, I. Králik⁵⁶, A. Kravčáková⁴⁰, M. Krivda^{56,104}, F. Krizek⁸⁶, E. Kryshen^{35,88}, M. Krzewicki⁴², A.M. Kubera¹⁹, V. Kučera⁸⁶, C. Kuhn⁶⁶, P.G. Kuijer⁸⁴, A. Kumar⁹³, J. Kumar⁴⁸, L. Kumar⁹⁰, S. Kumar⁴⁸, S. Kundu⁸¹, P. Kurashvili⁷⁹, A. Kurepin⁵³, A.B. Kurepin⁵³, A. Kuryakin¹⁰², S. Kushpil⁸⁶, M.J. Kweon⁵¹, Y. Kwon¹⁴², S.L. La Pointe⁴², P. La Rocca²⁸, C. Lagana Fernandes¹²³, I. Lakomov³⁵, R. Langoy⁴¹, K. Lapidus^{36,141}, C. Lara⁶⁰, A. Lardeux¹⁵, A. Lattuca²⁶, E. Laudi³⁵, L. Lazaridis³⁵, R. Lea²⁵, L. Leardini⁹⁶, S. Lee¹⁴², F. Lehas⁸⁴, S. Lehner¹¹⁵, J. Lehrbach⁴², R.C. Lemmon⁸⁵, V. Lenti¹⁰⁶, E. Leogrande⁵⁴, I. León Monzón¹²², P. Lévai¹⁴⁰, S. Li⁷, X. Li¹⁴, J. Lien⁴¹, R. Lietava¹⁰⁴, S. Lindal²¹, V. Lindenstruth⁴², C. Lippmann¹⁰⁰, M.A. Lisa¹⁹, H.M. Ljunggren³⁴, W. Llope¹³⁹, D.F. Lodato⁵⁴, P.I. Loenne²², V. Loginov⁷⁷, C. Loizides⁷⁶, X. Lopez⁷², E. López Torres⁹, A. Lowe¹⁴⁰, P. Luettig⁶¹, M. Lunardon²⁹, G. Luparello²⁵, M. Lupi³⁵, T.H. Lutz¹⁴¹, A. Maevskaya⁵³, M. Mager³⁵, S. Mahajan⁹³, S.M. Mahmood²¹, A. Maire⁶⁶, R.D. Majka¹⁴¹, M. Malaev⁸⁸, I. Maldonado Cervantes⁶³, L. Malinina^{68,iv}, D. Mal'Kevich⁵⁵, P. Malzacher¹⁰⁰, A. Mamonov¹⁰², V. Manko⁸², F. Manso⁷², V. Manzari¹⁰⁶, Y. Mao⁷, M. Marchisone^{130,67}, J. Mareš⁵⁷, G.V. Margagliotti²⁵, A. Margotti¹⁰⁷, J. Margutti⁵⁴, A. Marín¹⁰⁰, C. Markert¹²¹, M. Marquard⁶¹, N.A. Martin¹⁰⁰, P. Martinengo³⁵, M.I. Martínez², G. Martínez García¹¹⁶, M. Martinez Pedreira³⁵, A. Mas¹²³, S. Masciocchi¹⁰⁰, M. Masera²⁶, A. Masoni¹⁰⁸, A. Mastroserio³³, A. Matyja^{129,120}, C. Mayer¹²⁰, J. Mazer¹²⁹, M. Mazzilli³³, M.A. Mazzoni¹¹¹, F. Meddi²³, Y. Melikyan⁷⁷, A. Menchaca-Rocha⁶⁵, E. Meninno³⁰, J. Mercado Pérez⁹⁶, M. Meres³⁸, S. Mhlanga⁹², Y. Miake¹³², M.M. Mieskolainen⁴⁶, K. Mikhaylov^{55,68}, L. Milano⁷⁶, J. Milosevic²¹, A. Mischke⁵⁴, A.N. Mishra⁴⁹, T. Mishra⁵⁸, D. Miśkowiec¹⁰⁰, J. Mitra¹³⁷, C.M. Mitu⁵⁹, N. Mohammadi⁵⁴, B. Mohanty⁸¹, L. Molnar¹¹⁶, E. Montes¹⁰, D.A. Moreira De Godoy⁶², L.A.P. Moreno², S. Moretto²⁹, A. Morreale¹¹⁶, A. Morsch³⁵, V. Muccifora⁷⁴, E. Mudnic¹¹⁹, D. Mühlheim⁶², S. Muhuri¹³⁷, M. Mukherjee¹³⁷, J.D. Mulligan¹⁴¹, M.G. Munhoz¹²³, K. Müning⁴⁵, R.H. Munzer^{97,36,61}, H. Murakami¹³¹, S. Murray⁶⁷, L. Musa³⁵, J. Musinsky⁵⁶, C.J. Myers¹²⁶, B. Naik⁴⁸, R. Nair⁷⁹, B.K. Nandi⁴⁸, R. Nania¹⁰⁷, E. Nappi¹⁰⁶, M.U. Naru¹⁶, H. Natal da Luz¹²³, C. Natrass¹²⁹, S.R. Navarro², K. Nayak⁸¹, R. Nayak⁴⁸, T.K. Nayak¹³⁷, S. Nazarenko¹⁰², A. Nedosekin⁵⁵, R.A. Negrao De Oliveira³⁵, L. Nellen⁶³, F. Ng¹²⁶, M. Nicassio¹⁰⁰, M. Niculescu⁵⁹, J. Niedziela³⁵, B.S. Nielsen⁸³, S. Nikolaev⁸², S. Nikulin⁸², V. Nikulin⁸⁸, F. Noferini^{12,107}, P. Nomokonov⁶⁸, G. Nooren⁵⁴, J.C.C. Noris², J. Norman¹²⁸, A. Nyanin⁸², J. Nystrand²², H. Oeschler⁹⁶, S. Oh¹⁴¹, A. Ohlson³⁵, T. Okubo⁴⁷, L. Olah¹⁴⁰, J. Oleniacz¹³⁸, A.C. Oliveira Da Silva¹²³, M.H. Oliver¹⁴¹, J. Onderwaater¹⁰⁰, C. Oppedisano¹¹³, R. Orava⁴⁶, M. Oravec¹¹⁸, A. Ortiz Velasquez⁶³, A. Oskarsson³⁴, J. Otwinowski¹²⁰, K. Oyama⁷⁸, M. Ozdemir⁶¹, Y. Pachmayer⁹⁶, V. Pacik⁸³, D. Pagano^{26,135}, P. Pagano³⁰, G. Paic⁶³, S.K. Pal¹³⁷, P. Palni⁷, J. Pan¹³⁹, A.K. Pandey⁴⁸, V. Papikyan¹, G.S. Pappalardo¹⁰⁹, P. Pareek⁴⁹, J. Park⁵¹, W.J. Park¹⁰⁰, S. Parmar⁹⁰, A. Passfeld⁶², V. Paticchio¹⁰⁶, R.N. Patra¹³⁷, B. Paul¹¹³, H. Pei⁷, T. Peitzmann⁵⁴, X. Peng⁷, H. Pereira Da Costa¹⁵, D. Peresunko^{82,77}, E. Perez Lezama⁶¹, V. Peskov⁶¹, Y. Pestov⁵, V. Petráček³⁹, V. Petrov¹¹⁴, M. Petrovici⁸⁰, C. Petta²⁸, S. Piano¹¹², M. Pikna³⁸, P. Pillot¹¹⁶, L.O.D.L. Pimentel⁸³, O. Pinazza^{107,35}, L. Pinsky¹²⁶, D.B. Piyarathna¹²⁶, M. Płoskon⁷⁶, M. Planinic¹³³, J. Pluta¹³⁸, S. Pochybova¹⁴⁰, P.L.M. Podesta-Lerma¹²², M.G. Poghosyan⁸⁷, B. Polichtchouk¹¹⁴, N. Poljak¹³³, W. Poonsawat¹¹⁷, A. Pop⁸⁰, H. Poppenborg⁶², S. Porteboeuf-Houssais⁷², J. Porter⁷⁶, J. Pospisil⁸⁶, S.K. Prasad⁴, R. Preghenella^{107,35}, F. Prino¹¹³, C.A. Pruneau¹³⁹, I. Pshenichnov⁵³, M. Puccio²⁶, G. Puddu²⁴, P. Pujahari¹³⁹, V. Punin¹⁰², J. Putschke¹³⁹, H. Qvigstad²¹, A. Rachevski¹¹², S. Raha⁴, S. Rajput⁹³, J. Rak¹²⁷, A. Rakotozafindrabe¹⁵, L. Ramello³², F. Rami⁶⁶, D.B. Rana¹²⁶, R. Raniwala⁹⁴, S. Raniwala⁹⁴, S.S. Räsänen⁴⁶, B.T. Rascanu⁶¹, D. Rathee⁹⁰, V. Ratza⁴⁵, I. Ravasenga²⁶, K.F. Read^{129,87}, K. Redlich⁷⁹, A. Rehman²², P. Reichelt⁶¹, F. Reidt^{96,35}, X. Ren⁷, R. Renfordt⁶¹, A.R. Reolon⁷⁴, A. Reshetin⁵³, K. Reygers⁹⁶, V. Riabov⁸⁸, R.A. Ricci⁷⁵, T. Richert^{34,54}, M. Richter²¹, P. Riedler³⁵, W. Riegler³⁵, F. Riggi²⁸, C. Ristea⁵⁹, M. Rodríguez Cahuantzi², K. Røed²¹, E. Rogochaya⁶⁸, D. Rohr⁴², D. Röhrich²², F. Ronchetti^{74,35}, L. Ronflette¹¹⁶, P. Rosnet⁷², A. Rossi²⁹, F. Roukoutakis⁹¹, A. Roy⁴⁹, C. Roy⁶⁶, P. Roy¹⁰³, A.J. Rubio Montero¹⁰, R. Rui²⁵, R. Russo²⁶, E. Ryabinkin⁸²,

Y. Ryabov⁸⁸, A. Rybicki¹²⁰, S. Saarinen⁴⁶, S. Sadhu¹³⁷, S. Sadovsky¹¹⁴, K. Šafařík³⁵, B. Sahlmuller⁶¹,
 B. Sahoo⁴⁸, P. Sahoo⁴⁹, R. Sahoo⁴⁹, S. Sahoo⁵⁸, P.K. Sahu⁵⁸, J. Saini¹³⁷, S. Sakai^{132,74}, M.A. Saleh¹³⁹,
 J. Salzwedel¹⁹, S. Sambyal⁹³, V. Samsonov^{88,77}, A. Sandoval⁶⁵, M. Sano¹³², D. Sarkar¹³⁷, N. Sarkar¹³⁷,
 P. Sarma⁴⁴, M.H.P. Sas⁵⁴, E. Scapparone¹⁰⁷, F. Scarlassara²⁹, R.P. Scharenberg⁹⁸, C. Schiaua⁸⁰, R. Schicker⁹⁶,
 C. Schmidt¹⁰⁰, H.R. Schmidt⁹⁵, M. Schmidt⁹⁵, J. Schukraft³⁵, Y. Schutz^{35,66,116}, K. Schwarz¹⁰⁰,
 K. Schweda¹⁰⁰, G. Scioli²⁷, E. Scomparin¹¹³, R. Scott¹²⁹, M. Šefčík⁴⁰, J.E. Seger⁸⁹, Y. Sekiguchi¹³¹,
 D. Sekihata⁴⁷, I. Selyuzhenkov¹⁰⁰, K. Senosi⁶⁷, S. Senyukov^{3,35}, E. Serradilla^{10,65}, P. Sett⁴⁸, A. Sevcenco⁵⁹,
 A. Shabanov⁵³, A. Shabetai¹¹⁶, O. Shadura³, R. Shahoyan³⁵, A. Shangaraev¹¹⁴, A. Sharma⁹³, A. Sharma⁹⁰,
 M. Sharma⁹³, M. Sharma⁹³, N. Sharma^{90,129}, A.I. Sheikh¹³⁷, K. Shigaki⁴⁷, Q. Shou⁷, K. Shtejer^{26,9},
 Y. Sibiriak⁸², S. Siddhanta¹⁰⁸, K.M. Sielewicz³⁵, T. Siemiaczuk⁷⁹, D. Silvermyr³⁴, C. Silvestre⁷³,
 G. Simatovic¹³³, G. Simonetti³⁵, R. Singaraju¹³⁷, R. Singh⁸¹, V. Singhal¹³⁷, T. Sinha¹⁰³, B. Sitar³⁸, M. Sitta³²,
 T.B. Skaali²¹, M. Slupecki¹²⁷, N. Smirnov¹⁴¹, R.J.M. Snellings⁵⁴, T.W. Snellman¹²⁷, J. Song⁹⁹, M. Song¹⁴²,
 Z. Song⁷, F. Soramel²⁹, S. Sorensen¹²⁹, F. Sozzi¹⁰⁰, E. Spiriti⁷⁴, I. Sputowska¹²⁰, B.K. Srivastava⁹⁸, J. Stachel⁹⁶,
 I. Stan⁵⁹, P. Stankus⁸⁷, E. Stenlund³⁴, G. Steyn⁶⁷, J.H. Stiller⁹⁶, D. Stocco¹¹⁶, P. Strmen³⁸, A.A.P. Suaide¹²³,
 T. Sugitate⁴⁷, C. Suire⁵², M. Suleymanov¹⁶, M. Suljic²⁵, R. Sultanov⁵⁵, M. Šumbera⁸⁶, S. Sumowidagdo⁵⁰,
 K. Suzuki¹¹⁵, S. Swain⁵⁸, A. Szabo³⁸, I. Szarka³⁸, A. Szczepankiewicz¹³⁸, M. Szymanski¹³⁸, U. Tabassam¹⁶,
 J. Takahashi¹²⁴, G.J. Tambave²², N. Tanaka¹³², M. Tarhini⁵², M. Tariq¹⁸, M.G. Tarzila⁸⁰, A. Tauro³⁵, G. Tejeda
 Muñoz², A. Telesca³⁵, K. Terasaki¹³¹, C. Terrevoli²⁹, B. Teyssier¹³⁴, D. Thakur⁴⁹, D. Thomas¹²¹, R. Tieulent¹³⁴,
 A. Tikhonov⁵³, A.R. Timmins¹²⁶, A. Toia⁶¹, S. Tripathy⁴⁹, S. Trogolo²⁶, G. Trombetta³³, V. Trubnikov³,
 W.H. Trzaska¹²⁷, T. Tsuji¹³¹, A. Tumkin¹⁰², R. Turrisi¹¹⁰, T.S. Tveter²¹, K. Ullaland²², E.N. Umaka¹²⁶,
 A. Uras¹³⁴, G.L. Usai²⁴, A. Utrobitcic¹³³, M. Vala⁵⁶, J. Van Der Maarel⁵⁴, J.W. Van Hoorn³⁵, M. van
 Leeuwen⁵⁴, T. Vanat⁸⁶, P. Vande Vyvre³⁵, D. Varga¹⁴⁰, A. Vargas², M. Vargyas¹²⁷, R. Varma⁴⁸, M. Vasileiou⁹¹,
 A. Vasiliev⁸², A. Vauthier⁷³, O. Vázquez Doce^{97,36}, V. Vechernin¹³⁶, A.M. Veen⁵⁴, A. Velure²², E. Vercellin²⁶,
 S. Vergara Limón², R. Vernet⁸, R. Vértesi¹⁴⁰, L. Vickovic¹¹⁹, S. Vigolo⁵⁴, J. Viinikainen¹²⁷, Z. Vilakazi¹³⁰,
 O. Villalobos Baillie¹⁰⁴, A. Villatoro Tello², A. Vinogradov⁸², L. Vinogradov¹³⁶, T. Virgil³⁰, V. Vislavicius³⁴,
 A. Vodopyanov⁶⁸, M.A. Völkl⁹⁶, K. Voloshin⁵⁵, S.A. Voloshin¹³⁹, G. Volpe^{33,140}, B. von Haller³⁵,
 I. Vorobyev^{36,97}, D. Voscek¹¹⁸, D. Vranic^{35,100}, J. Vrláková⁴⁰, B. Wagner²², J. Wagner¹⁰⁰, H. Wang⁵⁴,
 M. Wang⁷, D. Watanabe¹³², Y. Watanabe¹³¹, M. Weber¹¹⁵, S.G. Weber¹⁰⁰, D.F. Weiser⁹⁶, J.P. Wessels⁶²,
 U. Westerhoff⁶², A.M. Whitehead⁹², J. Wiechula⁶¹, J. Wikne²¹, G. Wilk⁷⁹, J. Wilkinson⁹⁶, G.A. Willems⁶²,
 M.C.S. Williams¹⁰⁷, B. Windelband⁹⁶, M. Winn⁹⁶, S. Yalcin⁷¹, P. Yang⁷, S. Yano⁴⁷, Z. Yin⁷,
 H. Yokoyama^{73,132}, I.-K. Yoo^{35,99}, J.H. Yoon⁵¹, V. Yurchenko³, V. Zaccolo⁸³, A. Zaman¹⁶, C. Zampolli^{35,107},
 H.J.C. Zanolli¹²³, S. Zaporozhets⁶⁸, N. Zardoshti¹⁰⁴, A. Zarochentsev¹³⁶, P. Závada⁵⁷, N. Zaviyalov¹⁰²,
 H. Zbroszczyk¹³⁸, M. Zhalov⁸⁸, H. Zhang^{7,22}, X. Zhang^{76,7}, Y. Zhang⁷, C. Zhang⁵⁴, Z. Zhang⁷, C. Zhao²¹,
 N. Zhigareva⁵⁵, D. Zhou⁷, Y. Zhou⁸³, Z. Zhou²², H. Zhu^{22,7}, J. Zhu^{116,7}, A. Zichichi^{27,12}, A. Zimmermann⁹⁶,
 M.B. Zimmermann^{35,62}, G. Zinovjev³, J. Zmeskal¹¹⁵

Affiliation notes

ⁱ Deceased

ⁱⁱ Also at: Georgia State University, Atlanta, Georgia, United States

ⁱⁱⁱ Also at: Also at Department of Applied Physics, Aligarh Muslim University, Aligarh, India

^{iv} Also at: M.V. Lomonosov Moscow State University, D.V. Skobeltsyn Institute of Nuclear, Physics, Moscow, Russia

Collaboration Institutes

¹A.I. Alikhanyan National Science Laboratory (Yerevan Physics Institute) Foundation, Yerevan, Armenia

²Benemérita Universidad Autónoma de Puebla, Puebla, Mexico

³Bogolyubov Institute for Theoretical Physics, Kiev, Ukraine

⁴Bose Institute, Department of Physics and Centre for Astroparticle Physics and Space Science (CAPSS), Kolkata, India

⁵Budker Institute for Nuclear Physics, Novosibirsk, Russia

⁶California Polytechnic State University, San Luis Obispo, California, United States

⁷Central China Normal University, Wuhan, China

⁸Centre de Calcul de l'IN2P3, Villeurbanne, Lyon, France

⁹Centro de Aplicaciones Tecnológicas y Desarrollo Nuclear (CEADEN), Havana, Cuba

- ¹⁰Centro de Investigaciones Energéticas Medioambientales y Tecnológicas (CIEMAT), Madrid, Spain
¹¹Centro de Investigación y de Estudios Avanzados (CINVESTAV), Mexico City and Mérida, Mexico
¹²Centro Fermi - Museo Storico della Fisica e Centro Studi e Ricerche “Enrico Fermi”, Rome, Italy
¹³Chicago State University, Chicago, Illinois, United States
¹⁴China Institute of Atomic Energy, Beijing, China
¹⁵Commissariat à l’Energie Atomique, IRFU, Saclay, France
¹⁶COMSATS Institute of Information Technology (CIIT), Islamabad, Pakistan
¹⁷Departamento de Física de Partículas and IGFAE, Universidad de Santiago de Compostela, Santiago de Compostela, Spain
¹⁸Department of Physics, Aligarh Muslim University, Aligarh, India
¹⁹Department of Physics, Ohio State University, Columbus, Ohio, United States
²⁰Department of Physics, Sejong University, Seoul, South Korea
²¹Department of Physics, University of Oslo, Oslo, Norway
²²Department of Physics and Technology, University of Bergen, Bergen, Norway
²³Dipartimento di Fisica dell’Università ‘La Sapienza’ and Sezione INFN, Rome, Italy
²⁴Dipartimento di Fisica dell’Università and Sezione INFN, Cagliari, Italy
²⁵Dipartimento di Fisica dell’Università and Sezione INFN, Trieste, Italy
²⁶Dipartimento di Fisica dell’Università and Sezione INFN, Turin, Italy
²⁷Dipartimento di Fisica e Astronomia dell’Università and Sezione INFN, Bologna, Italy
²⁸Dipartimento di Fisica e Astronomia dell’Università and Sezione INFN, Catania, Italy
²⁹Dipartimento di Fisica e Astronomia dell’Università and Sezione INFN, Padova, Italy
³⁰Dipartimento di Fisica ‘E.R. Caianiello’ dell’Università and Gruppo Collegato INFN, Salerno, Italy
³¹Dipartimento DISAT del Politecnico and Sezione INFN, Turin, Italy
³²Dipartimento di Scienze e Innovazione Tecnologica dell’Università del Piemonte Orientale and INFN Sezione di Torino, Alessandria, Italy
³³Dipartimento Interateneo di Fisica ‘M. Merlin’ and Sezione INFN, Bari, Italy
³⁴Division of Experimental High Energy Physics, University of Lund, Lund, Sweden
³⁵European Organization for Nuclear Research (CERN), Geneva, Switzerland
³⁶Excellence Cluster Universe, Technische Universität München, Munich, Germany
³⁷Faculty of Engineering, Bergen University College, Bergen, Norway
³⁸Faculty of Mathematics, Physics and Informatics, Comenius University, Bratislava, Slovakia
³⁹Faculty of Nuclear Sciences and Physical Engineering, Czech Technical University in Prague, Prague, Czech Republic
⁴⁰Faculty of Science, P.J. Šafárik University, Košice, Slovakia
⁴¹Faculty of Technology, Buskerud and Vestfold University College, Tønsberg, Norway
⁴²Frankfurt Institute for Advanced Studies, Johann Wolfgang Goethe-Universität Frankfurt, Frankfurt, Germany
⁴³Gangneung-Wonju National University, Gangneung, South Korea
⁴⁴Gauhati University, Department of Physics, Guwahati, India
⁴⁵Helmholtz-Institut für Strahlen- und Kernphysik, Rheinische Friedrich-Wilhelms-Universität Bonn, Bonn, Germany
⁴⁶Helsinki Institute of Physics (HIP), Helsinki, Finland
⁴⁷Hiroshima University, Hiroshima, Japan
⁴⁸Indian Institute of Technology Bombay (IIT), Mumbai, India
⁴⁹Indian Institute of Technology Indore, Indore, India
⁵⁰Indonesian Institute of Sciences, Jakarta, Indonesia
⁵¹Inha University, Incheon, South Korea
⁵²Institut de Physique Nucléaire d’Orsay (IPNO), Université Paris-Sud, CNRS-IN2P3, Orsay, France
⁵³Institute for Nuclear Research, Academy of Sciences, Moscow, Russia
⁵⁴Institute for Subatomic Physics of Utrecht University, Utrecht, Netherlands
⁵⁵Institute for Theoretical and Experimental Physics, Moscow, Russia
⁵⁶Institute of Experimental Physics, Slovak Academy of Sciences, Košice, Slovakia
⁵⁷Institute of Physics, Academy of Sciences of the Czech Republic, Prague, Czech Republic
⁵⁸Institute of Physics, Bhubaneswar, India
⁵⁹Institute of Space Science (ISS), Bucharest, Romania
⁶⁰Institut für Informatik, Johann Wolfgang Goethe-Universität Frankfurt, Frankfurt, Germany
⁶¹Institut für Kernphysik, Johann Wolfgang Goethe-Universität Frankfurt, Frankfurt, Germany

- ⁶²Institut für Kernphysik, Westfälische Wilhelms-Universität Münster, Münster, Germany
⁶³Instituto de Ciencias Nucleares, Universidad Nacional Autónoma de México, Mexico City, Mexico
⁶⁴Instituto de Física, Universidade Federal do Rio Grande do Sul (UFRGS), Porto Alegre, Brazil
⁶⁵Instituto de Física, Universidad Nacional Autónoma de México, Mexico City, Mexico
⁶⁶Institut Pluridisciplinaire Hubert Curien (IPHC), Université de Strasbourg, CNRS-IN2P3, Strasbourg, France, Strasbourg, France
⁶⁷iThemba LABS, National Research Foundation, Somerset West, South Africa
⁶⁸Joint Institute for Nuclear Research (JINR), Dubna, Russia
⁶⁹Konkuk University, Seoul, South Korea
⁷⁰Korea Institute of Science and Technology Information, Daejeon, South Korea
⁷¹KTO Karatay University, Konya, Turkey
⁷²Laboratoire de Physique Corpusculaire (LPC), Clermont Université, Université Blaise Pascal, CNRS-IN2P3, Clermont-Ferrand, France
⁷³Laboratoire de Physique Subatomique et de Cosmologie, Université Grenoble-Alpes, CNRS-IN2P3, Grenoble, France
⁷⁴Laboratori Nazionali di Frascati, INFN, Frascati, Italy
⁷⁵Laboratori Nazionali di Legnaro, INFN, Legnaro, Italy
⁷⁶Lawrence Berkeley National Laboratory, Berkeley, California, United States
⁷⁷Moscow Engineering Physics Institute, Moscow, Russia
⁷⁸Nagasaki Institute of Applied Science, Nagasaki, Japan
⁷⁹National Centre for Nuclear Studies, Warsaw, Poland
⁸⁰National Institute for Physics and Nuclear Engineering, Bucharest, Romania
⁸¹National Institute of Science Education and Research, Bhubaneswar, India
⁸²National Research Centre Kurchatov Institute, Moscow, Russia
⁸³Niels Bohr Institute, University of Copenhagen, Copenhagen, Denmark
⁸⁴Nikhef, Nationaal instituut voor subatomaire fysica, Amsterdam, Netherlands
⁸⁵Nuclear Physics Group, STFC Daresbury Laboratory, Daresbury, United Kingdom
⁸⁶Nuclear Physics Institute, Academy of Sciences of the Czech Republic, Řež u Prahy, Czech Republic, Řež u Prahy, Czech Republic
⁸⁷Oak Ridge National Laboratory, Oak Ridge, Tennessee, United States
⁸⁸Petersburg Nuclear Physics Institute, Gatchina, Russia
⁸⁹Physics Department, Creighton University, Omaha, Nebraska, United States
⁹⁰Physics Department, Panjab University, Chandigarh, India
⁹¹Physics Department, University of Athens, Athens, Greece
⁹²Physics Department, University of Cape Town, Cape Town, South Africa
⁹³Physics Department, University of Jammu, Jammu, India
⁹⁴Physics Department, University of Rajasthan, Jaipur, India
⁹⁵Physikalisches Institut, Eberhard Karls Universität Tübingen, Tübingen, Germany
⁹⁶Physikalisches Institut, Ruprecht-Karls-Universität Heidelberg, Heidelberg, Germany
⁹⁷Physik Department, Technische Universität München, Munich, Germany
⁹⁸Purdue University, West Lafayette, Indiana, United States
⁹⁹Pusan National University, Pusan, South Korea
¹⁰⁰Research Division and ExtreMe Matter Institute EMMI, GSI Helmholtzzentrum für Schwerionenforschung, Darmstadt, Germany
¹⁰¹Rudjer Bošković Institute, Zagreb, Croatia
¹⁰²Russian Federal Nuclear Center (VNIIEF), Sarov, Russia
¹⁰³Saha Institute of Nuclear Physics, Kolkata, India
¹⁰⁴School of Physics and Astronomy, University of Birmingham, Birmingham, United Kingdom
¹⁰⁵Sección Física, Departamento de Ciencias, Pontificia Universidad Católica del Perú, Lima, Peru
¹⁰⁶Sezione INFN, Bari, Italy
¹⁰⁷Sezione INFN, Bologna, Italy
¹⁰⁸Sezione INFN, Cagliari, Italy
¹⁰⁹Sezione INFN, Catania, Italy
¹¹⁰Sezione INFN, Padova, Italy
¹¹¹Sezione INFN, Rome, Italy
¹¹²Sezione INFN, Trieste, Italy

- ¹¹³Sezione INFN, Turin, Italy
¹¹⁴SSC IHEP of NRC Kurchatov institute, Protvino, Russia
¹¹⁵Stefan Meyer Institut für Subatomare Physik (SMI), Vienna, Austria
¹¹⁶SUBATECH, Ecole des Mines de Nantes, Université de Nantes, CNRS-IN2P3, Nantes, France
¹¹⁷Suranaree University of Technology, Nakhon Ratchasima, Thailand
¹¹⁸Technical University of Košice, Košice, Slovakia
¹¹⁹Technical University of Split FESB, Split, Croatia
¹²⁰The Henryk Niewodniczanski Institute of Nuclear Physics, Polish Academy of Sciences, Cracow, Poland
¹²¹The University of Texas at Austin, Physics Department, Austin, Texas, United States
¹²²Universidad Autónoma de Sinaloa, Culiacán, Mexico
¹²³Universidade de São Paulo (USP), São Paulo, Brazil
¹²⁴Universidade Estadual de Campinas (UNICAMP), Campinas, Brazil
¹²⁵Universidade Federal do ABC, Santo Andre, Brazil
¹²⁶University of Houston, Houston, Texas, United States
¹²⁷University of Jyväskylä, Jyväskylä, Finland
¹²⁸University of Liverpool, Liverpool, United Kingdom
¹²⁹University of Tennessee, Knoxville, Tennessee, United States
¹³⁰University of the Witwatersrand, Johannesburg, South Africa
¹³¹University of Tokyo, Tokyo, Japan
¹³²University of Tsukuba, Tsukuba, Japan
¹³³University of Zagreb, Zagreb, Croatia
¹³⁴Université de Lyon, Université Lyon 1, CNRS/IN2P3, IPN-Lyon, Villeurbanne, Lyon, France
¹³⁵Università di Brescia, Brescia, Italy
¹³⁶V. Fock Institute for Physics, St. Petersburg State University, St. Petersburg, Russia
¹³⁷Variable Energy Cyclotron Centre, Kolkata, India
¹³⁸Warsaw University of Technology, Warsaw, Poland
¹³⁹Wayne State University, Detroit, Michigan, United States
¹⁴⁰Wigner Research Centre for Physics, Hungarian Academy of Sciences, Budapest, Hungary
¹⁴¹Yale University, New Haven, Connecticut, United States
¹⁴²Yonsei University, Seoul, South Korea
¹⁴³Zentrum für Technologietransfer und Telekommunikation (ZTT), Fachhochschule Worms, Worms, Germany